Amplitude collapse of nonlinear double-layer oscillations

M. Wendt, I. Axnäs, and S. Torvén
Division of Plasma Physics, Alfvén Laboratory, SE-100 44 Stockholm, Sweden
(Received 25 September 1997)

The negative differential resistance of a double layer can give rise to large amplitude oscillations in the potential drop over the double layer. Such oscillations are investigated in a triple-plasma machine for weak nonlinearity, implying approximately harmonic oscillations at low frequencies ($\omega \ll \omega_{pi}$). The amplitude of the potential oscillations can approach the dc potential drop over the double layer. The oscillation exists within a certain interval of dc drops and vanishes outside this interval. An interesting nonlinear phenomenon that we call amplitude collapse is observed. The amplitude does not always decrease smoothly from its maximum value to zero when the dc drop is increased, but there is a sudden jump to vanishing amplitudes. For a decreasing dc voltage the corresponding sharp amplitude increase occurs at a lower voltage. This phenomenon, which is not predicted by the classical van der Pol equation, is shown to follow from the generalized van der Pol equation that describes the actual system, by using asymptotic solutions for weak nonlinearity. [S1063-651X(98)03804-5]

PACS number(s): 52.40.Hf, 52.35.Fp

I. INTRODUCTION

Oscillations at frequencies far below the ion plasma frequency often occur in bounded, current-carrying plasmas [1–5]. Usually all relevant plasma parameters oscillate and give rise to oscillations in the electric current and the potential drop over the plasma, and there may be a complicated interaction between the plasma and the external electric circuit. In particular, experiments in a triple-plasma machine have shown that such oscillations can be excited by the negative differential resistance of strong electric double layers [6]. For strong nonlinearity and a sufficiently inductive current circuit, the oscillations assume the form of sharp current disruptions giving high inductive voltage drops that are supported by the double layer [7]. In a more recent experiment, the system was investigated when a periodic driver signal was added to the self-excited oscillations [8]. A simplified model for the negative differential resistance of the double layer in the triple-plasma machine was also presented. It is based on the existence of a current-limiting potential minimum at the low potential side of the double layer. This potential minimum decreases with increasing double-layer potential drop, which results in a decreasing current due to the reflection of the current-carrying electrons. A model equation in the form of a generalized van der Pol equation was proposed, based on the static current-voltage characteristic. The addition of a periodic driver signal results in an enriched dynamical behavior including frequency entrainment, quasiperiodicity, periodic pulling, and period-doubling bifurcations, in agreement with the known bifurcation structure of the periodically driven van der Pol oscillator [9–11]. The van der Pol equation has already been applied to related oscillatory phenomena in bounded plasmas [12–15] and electronic circuits [16].

In this paper we investigate self-oscillations of a double layer when the nonlinear perturbation is small during one oscillation period and the nonlinearity is accordingly weak. The potential oscillations are then approximately harmonic with a frequency determined by the resonance frequency of the current circuit, and they have low frequency so that the static current-voltage characteristic is valid. The measurements were performed using a triple-plasma machine at the Royal Institute of Technology. We present potential profiles of the oscillating double layer and amplitude characteristics, that is, the oscillation amplitude as a function of the dc potential drop over the double layer. Some preliminary results have been published in a conference paper [17]. The oscillations exist within a certain interval of dc drops; this is correlated with the interval of negative differential resistance in the current-voltage characteristic, and they vanish outside this interval. The amplitude of the stationary oscillation is varied by changing the parameters of the external circuit. For small amplitudes there is a smooth amplitude variation in agreement with predictions from the classical van der Pol equation [18]. However, for larger amplitudes a new phenomenon appears (amplitude collapse). It is characterized by sharp amplitude jumps and hysteresis at certain dc voltages. This behavior is not predicted by the classical van der Pol equation. A similar collapse was noted in the behavior of an electronic circuit [16]. To interpret the results we consider solutions of the generalized van der Pol equation obtained for the measured static current-voltage characteristic. Solutions given by an asymptotic method for weak nonlinearity are used [19]. The theoretical amplitude characteristics show good agreement with the measured ones and, in particular, the amplitude collapse and the hysteresis are predicted by theory. A condition for the existence of the hysteresis in terms of the static differential conductance of the plasma is also given.

II. EXPERIMENTAL DEVICE AND THE CURRENT CIRCUIT

The triple-plasma machine and the electric circuit are shown in Fig. 1. In the chambers S_1 and S_2, independent discharges between heated tungsten filaments and the chamber walls take place. Their power supplies are fed from isolation transformers so that both sources can be operated with

 © 1998 The American Physical Society

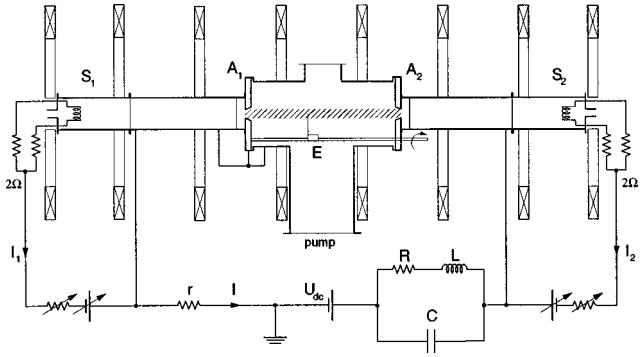

FIG. 1. Schematic picture of the triple-plasma machine and the external circuit. The plasma column in the central chamber is maintained by plasma diffusing from the sources S_1 and S_2. A magnetic field $B=13$ mT confines the plasma radially. R is the resistance of the inductor.

a high impedance to ground. S_1 and S_2 connect to the central chamber through electrically isolated circular apertures in the end plates of the central chamber. The aperture diameter (3 cm) determines the diameter of the plasma column in the central chamber. The plasma is confined radially by a homogeneous magnetic field ($B=13$ mT). Since the aperture diameter is small compared to the diffusion pump diameter (25 cm), it is possible to maintain sufficiently high neutral argon pressure in the sources (20 mPa) to obtain low voltage discharges while simultaneously the neutral gas density in the central chamber is typically an order of magnitude smaller. In this manner, ionization by electron impacts is suppressed in the central chamber. The particle injection from the sources is electron rich, and electron-reflecting potential drops of the order of k_BT_e/e develop at the apertures. The discharge parameters used for S_1 are discharge voltage 35.0 V and discharge current 1.7 A, and for S_2 are discharge voltage 28.1 V and discharge current 1.7 A. In the plasma column we have $n_e=2\times10^{15}$ m^{-3}, $T_e=8$ eV, $\omega_{pe}=2.5\times10^9$ rad/s, and $\omega_{pi}=9.3\times10^6$ rad/s.

When a steady voltage drop U_0, exceeding about k_BT_e/e, is applied between source chamber walls, a double layer forms in the central chamber. The potential drop U_{DL} over the double layer is determined by

$$U_0=U_{\mathrm{DL}}+U_p+U_s, \tag{1}$$

where U_p is the small potential drop in the plasma column, outside the double-layer region, and U_s is the potential drop due to any difference between the two source plasmas. If these were identical, U_s would vanish.

The current $I(t)$ between the sources is measured as the voltage drop across the small resistor $r=10\,\Omega$, which couples S_1 to ground. $I(t)$ is the current passing through the right aperture and the double layer because the left end plate and the central chamber are not grounded, but rather connected to the chamber wall of S_1.

The external circuit is a parallel LC circuit according to Fig. 1. For the potential drop $U(t)$ between the source anodes it holds that

$$LC\frac{d^2}{dt^2}U+RC\frac{d}{dt}U+L\frac{d}{dt}I+U=U_{\mathrm{dc}}, \tag{2}$$

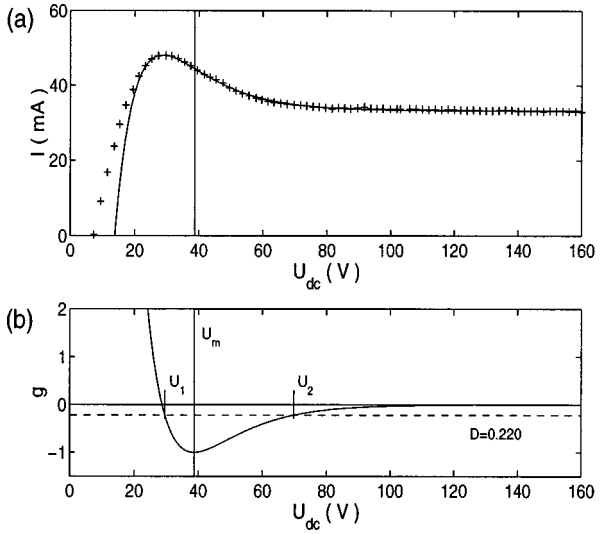

FIG. 2. (a) Experimental current-voltage characteristic of the triple-plasma machine (+). The solid curve is the least-squares fit to I derived in Sec. IV. (b) Differential conductance $g(U_{\mathrm{dc}})$, according to Eq. (14) with least-squares fit values $V_1=14.6$ V, $V_2=7.2$ V, and $U_m=38.7$ V obtained for the experimental data. The dashed line gives the zero level of $g(U_{\mathrm{dc}})+D$ for $D=0.220$. Small-amplitude fluctuations grow exponentially if U_{dc} is in the interval (U_1,U_2), where $g(U_{\mathrm{dc}})+D<0$.

where L and C are the inductance and the capacitance and R is the resistance of the inductor. The resistive voltage drops across r and R (≈0.2 V) are neglected since they are much smaller than U. However, the term $RC(d/dt)U$ cannot be neglected because it is essential for the understanding of the amplitude collapse, as shown below. Introducing the static current-voltage characteristic $I(U)$ we have

$$\frac{d}{dt}I=I'(U)\frac{d}{dt}U, \tag{3}$$

where $'$ means the derivative with respect to U. Figure 2 shows the static current-voltage characteristic valid for the measurements and the analytical fit described below. $I'(U)$ is negative in a certain region and it assumes a minimum value for $U=U_m$. It is convenient to set $I'(U_m)=-1/R_m$ and work with the normalized conductance $g(U)=R_mI'(U)$, so that $g(U_m)=-1$ [Fig. 2(b)]. Introducing $V=U-U_{\mathrm{dc}}$ and normalizing the time by setting $\tau=t/\sqrt{LC}$, we get the equation

$$\frac{d^2}{d\tau^2}V+V=-\epsilon[g(V+U_{\mathrm{dc}})+D]\frac{d}{d\tau}V. \tag{4}$$

The coefficients ϵ and D are defined as

$$\epsilon=\frac{1}{R_m}\sqrt{\frac{L}{C}}\quad\text{and}\quad D=\frac{R}{R_m\epsilon^2}=\frac{RR_mC}{L}, \tag{5}$$

and represent the nonlinear coupling coefficient and the damping coefficient of the external circuit. Although we have $R\ll R_m$, the damping D is important when $\epsilon\ll1$ so that ϵ^2 is of the order of R/R_m. When $V+U_{\mathrm{dc}}$ is large, the damping is also important for any value of ϵ since g vanishes for large values of its argument.

TABLE I. Experimental parameters: external capacitance C and measured oscillation frequency f. f deviates only 1% from $1/(2\pi\sqrt{LC})$, with $L=60.8$ mH. R is the resistance of the inductor at frequency f. The nonlinearity coefficient ϵ and damping coefficient D follow from Eq. (5) with $R_m=(1950\pm100)\Omega$. The error in ϵ and D is 5%.

C (μF)	f (rad/s)	R (Ω)	ϵ	D
1	646	6.87	0.126	0.220
2	457	5.18	0.089	0.333
3	374	4.62	0.073	0.445
4	326	4.34	0.063	0.557
5	290	4.17	0.057	0.669
6	266	4.06	0.052	0.781
7	246	3.98	0.048	0.893
8	230	3.92	0.045	1.005

Equation (4) is a generalized van der Pol equation. It can be reduced to the classical van der Pol equation only when $U_{\rm dc}=U_m$ and V is small so that $g(V+U_m)$ can be approximated by a parabola in V. In this case the amplitude characteristic is given by Eq. (16) below. One stationary solution of Eq. (4) is $V=0$ (where $g''(U_{\rm dc})$ is positive). When $D>1$ this solution is stable for all values of $U_{\rm dc}$. When $D<1$, there is an interval (U_1, U_2) around U_m where $g(U_{\rm dc})+D<0$ and small fluctuations in V grow exponentially. For D close to unity, this interval becomes small so that a parabolic approximation for $g(U_{\rm dc})$ becomes valid.

With a suitable choice of L and C, high-resonance frequencies and small nonlinearity can be reached simultaneously. However, for higher-oscillation frequencies than those presented here, the static current-voltage approach is not valid. For a comparison between experiment and theory, a model including the ion dynamics would be needed.

III. EXPERIMENTS

To obtain weak nonlinearity ($\epsilon\ll1$), low-oscillation frequencies, and a well-defined resonance frequency $f_0=1/(2\pi\sqrt{LC})$, we have chosen $L=60.8$ mH and values of the capacitance C according to Table I. To avoid any saturation effects, an inductor without an iron core is used. In a separate experiment the frequency dependence of the inductance L and its resistance R is determined. The inductor is put in a series RLC circuit and the admittance $|I/U|$ of this circuit is measured for different, well-known capacitances C_1 ($\pm0.5\%$). Least-squares fits of the theoretical form of the admittance give the resistance R and the inductance L of the coil as a function of frequency. Whereas L remains constant within 0.4% up to a frequency of 600 Hz, R shows a parabolic increase due to eddy currents induced by the magnetic field in the coil (Fig. 3). At 600 Hz R has increased to 160% of its dc value. Fitting R to a second-order polynomial in f gives $R=(8.08\times10^{-6}f^2+2.71\times10^{-3}f+3.49)\Omega$, where f is in Hz. In the following this approximation is used. Table I shows next to R the corresponding values of ϵ and the damping coefficient D. The variation of R with the frequency has to be taken into account for a quantitative comparison between measurement and theory.

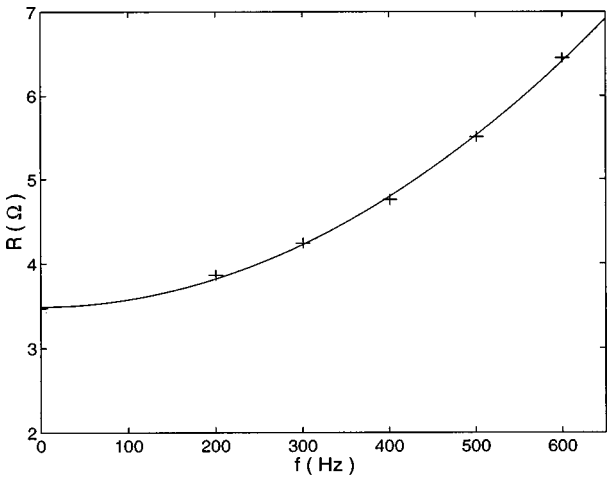

FIG. 3. Resistance R of the inductor used. R increases with f due to eddy currents induced by the magnetic field in the coil. R has been obtained from the resonance curve of a series RLC circuit for different, well-known capacitances. The solid line is the parabolic least-squares fit $R=(8.08\times10^{-6}f^2+2.71\times10^{-3}f+3.49)\Omega$, f in Hz.

Figure 4 shows the voltage drop U between the sources, the electric current I passing the double layer, and the corresponding time variation of the potential minimum or ''virtual cathode,'' that forms typically 5–10 cm from aperture A_1. In the case considered, $C=5$ μF. Figure 4(b) shows the potential variation along the axis of the plasma column at four different times marked in Fig. 4(a). The profiles show the small potential variation on the low-potential side of the double layer that gives rise to the variation of the virtual cathode potential. Figure 4(c) includes the double layer in the profiles. When the voltage drop is low ($t=t_1$) the double layer does not form, except for $t=t_2$. Here, a weak potential minimum is also present at the foot of the double layer with a level well above the virtual cathode potential. When the double layer becomes strong, so that $eU_{\rm DL}\gg k_BT_e$ (t_3 and t_4), the minimum at the foot of the double layer disappears. This is in agreement with the prediction from the one-dimensional Vlasow-Poisson system that strong double layers with foot-point minima do not exist. Such triple layers exist only when $eU_{\rm DL}$ is of the order of k_BT_e or lower [20].

The current limitation is caused by the virtual cathode. This forms because the plasma from S_1 is injected under ''electron-rich'' conditions, that is, the potential drop of the order of k_BT_e, which develops at the aperture A_1, accelerates source ions into the central chamber and reflects some of the source electrons. In the plasma region between the virtual cathode and the double layer, a weak electric field accelerates the electrons. Such a pre-acceleration is expected because the generalized Bohm condition for the electrons must be fulfilled at the double layer [21]. In experiments in a ''double-ended'' Q machine under electron-rich conditions, the virtual cathode associated with a dynamic double layer has also been observed to form close to the low-potential electrode, and a plasma region, pre-accelerating the electrons as observed in our experiment, separated the double layer and the virtual cathode [22].

According to a model proposed elsewhere [6,8], the double layer controls the depth of the virtual cathode in the

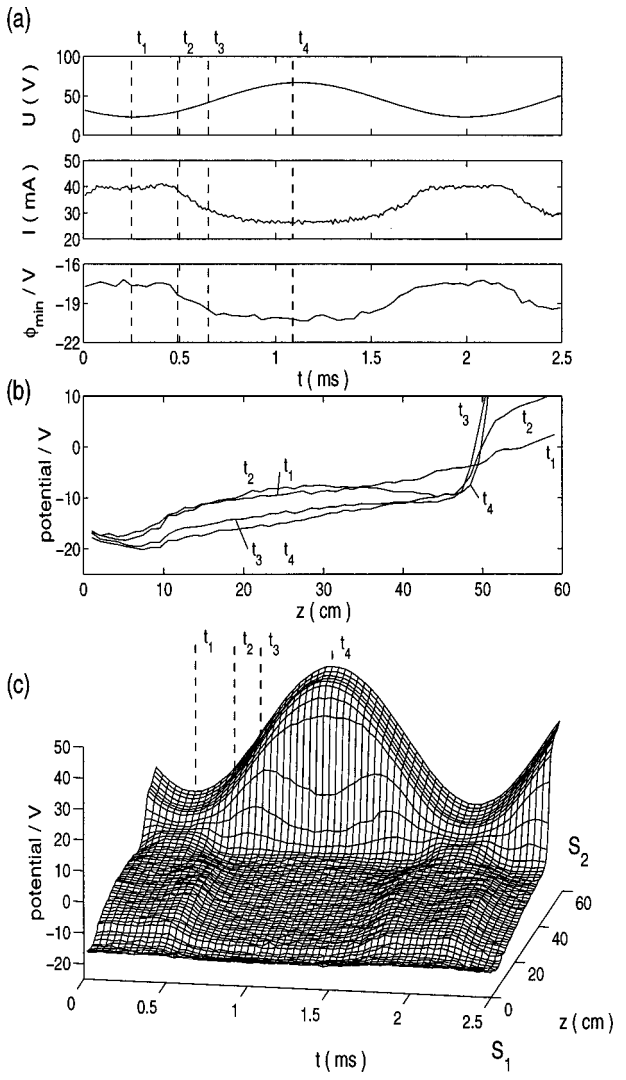

FIG. 4. (a) Voltage and current oscillation at $C=5\,\mu$F, $U_{dc}=45$ V. The oscillation of the voltage is closely harmonic with $f=574$ Hz. Hysteresis effects in the current can be neglected so that the static current-voltage characteristic (Fig. 2) can be used. The current I across the double layer is limited by the virtual cathode ϕ_{min} near aperture A_1. (b) Potential profiles. z is the coordinate along the plasma column. The sheaths near the apertures are not shown. When the potential difference between S_1 and S_2 is high, a strong double layer forms near aperture A_2. For small potential differences an additional potential dip exists near the foot of the double layer, but has a level well above the virtual cathode ($t=t_2$). (c) Time- and space-resolved plasma potential profile.

following manner: During the phase when U_{DL} is increasing and simultaneously, $eU_{DL}\gg k_BT_e$, the contribution from S_2 to the electron density in the plasma on the low-potential side is negligible. The contribution of S_2 to the ion number density there decreases, since the ions are accelerated in the increasing double-layer drop and enter the plasma region with increasing velocity. To maintain quasineutrality in the plasma region, the particle fluxes from S_1 must accordingly change so that the ion number density contribution increases relative to the electron number density contribution. This occurs when the virtual cathode potential decreases. Then the contribution to the electron density decreases strongly since the electron flux from S_1 is attenuated approximately according to the Boltzmann relation. The corresponding contribution to the ion density decreases much more slowly, since its decrease is only due to the velocity change when the source ions are accelerated into the central chamber. In the present case, this mechanism controls the virtual cathode level at some time $t>t_2$ when the double layer becomes strong. As long as the double layer is weak, the virtual cathode by itself does not control the current, because the current also increases due to an increasing reflection of electrons from S_2. The change of the virtual cathode potential between t_2 and t_4 is 2 V [Fig. 4(a)]. For $T_e=8$ eV the Boltzmann relation gives a relative electron density decrease of 22%. The relative current drop between t_2 and t_4 is 31%. The measured current decrease is larger because the double layer still may not be sufficiently strong at t_2 and a small electron-density contribution from S_2 may remain at the virtual cathode.

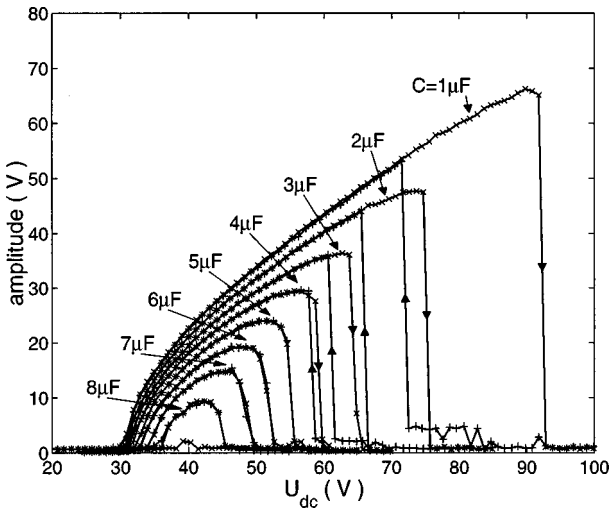

FIG. 5. Measured amplitudes at slowly varying dc voltage U_{dc} (+, increasing; ×, decreasing). For high capacitances the amplitude characteristics have approximately the same shape as predicted by the classical van der Pol equation. The sudden collapses of the double-layer oscillation and the hysteresis for $C\leqslant 4\,\mu$F can be understood from asymptotic solutions of the generalized van der Pol equation used here.

The virtual cathode decreases very slowly with increasing U_{DL} when U_{DL} is higher than about 100 V, and its control by the double layer finally ceases. This corresponds to the vanishing I' in the static current-voltage characteristic [Fig. 2(a)]. It is likely that the ion-density contribution from S_2, compared to the contribution from S_1 and the trapped ion density, then becomes too small to control the virtual cathode. A trapped ion population exists on the low-potential side of the double layer, because the radial electric field is inward there, in contrast to the plasma on the high-potential side, where it is outward. The trapped ion density is maintained by a balance between radial ion losses and trapping due to charge-exchange collisions and electron-impact ionization.

Figure 5 shows the voltage oscillation amplitudes (peak values averaged over ten trigger events) for different capacitances C at slowly varying dc voltage U_{dc}. The power supplies for filament heating and discharge current and the secondary winding of the isolation transformer of S_2 give rise to a stray capacitance of approximately 1.5 nF [8]. In comparison to the external capacitances C used here, this can be

neglected. As seen from Table I, the conditions required for weak nonlinearity are reasonably fulfilled. The measured voltage oscillation is approximately harmonic [Fig. 4(a)] and its frequency agrees with the resonance frequency $1/(2\pi\sqrt{LC})$ within 1%, as required by the asymptotic solution used below. For $C=7\ \mu$F ($D=0.89$), the maximum oscillation amplitude is of the order of $k_B T_e/e$. Since D is close to unity, this characteristic has approximately the same shape as known from the van der Pol oscillator. With decreasing capacitance the amplitudes get higher and the shapes of the characteristics become more asymmetric. For capacitances smaller than 4 μF ($D<0.75$) the amplitude characteristic shows a hysteresis phenomenon. With increasing $U_{\rm dc}$ the oscillation suddenly disappears shortly after having gone through its maximum value. At $C=1\ \mu$F the maximum amplitude becomes 74% of the dc voltage $U_{\rm dc}$. With decreasing $U_{\rm dc}$, the dc voltage at which the double layer becomes unstable and the voltage oscillation appears again, occurs at lower values, so that the amplitude undergoes a hysteresis. Its width increases with decreasing C and D.

IV. THEORY

To clarify the dependency of the oscillation amplitude on the dc voltage $U_{\rm dc}$, and especially the hysteresis, we apply the method of Bogoliubov and Mitropolsky [19]. With their method it is possible to derive approximate solutions for differential equations of the form

$$\frac{d^2}{dt^2}V+\omega^2 V=\epsilon h\left(V,\frac{d}{dt}V\right), \tag{6}$$

where ϵ is small ($\epsilon\ll 1$). The solution $V(t)$ is expanded in the form

$$V=a(t)\cos\,\psi(t)+\epsilon u_1(a,\psi)+\epsilon^2 u_2(a,\psi)+\cdots, \tag{7}$$

where the momentary amplitude $a(t)$ and phase $\psi(t)$ are determined by the differential equations

$$\frac{d}{dt}a=\epsilon A_1(a)+\epsilon^2 A_2(a)+\cdots, \tag{8}$$

$$\frac{d}{dt}\psi=\omega+\epsilon B_1(a)+\epsilon_2 B_2(a)+\cdots. \tag{9}$$

All functions $A_n(a)$, $B_n(a)$, and $u_n(a,\psi)$ can successively be determined. In the first-order approximation, considered here, u_1 and all terms containing ϵ^2 and higher orders of ϵ are neglected. $B_1(a)$ equals zero in our case, because $h(V,dV/dt)$ has the form of a nonlinear damping, so that $d\psi/dt=\omega$. It follows that the frequency of $V(t)$ is given by $1/(2\pi\sqrt{LC})$, which is in close agreement with the experiment. Applied to Eq. (4), we get

$$V=a(\tau)\cos\,\psi,\quad \dot{a}=\epsilon A_1(a), \tag{10}$$

where the dot denotes derivative with respect to τ. $A_1(a)$ is given by

$$A_1(a)=-\frac{1}{2\pi}\int_0^{2\pi}[g(a\,\cos\,\psi+U_{\rm dc})+D]a\,\sin^2\,\psi\,d\psi. \tag{11}$$

Stationary solutions ($\dot{a}=0$) are determined by the roots of $A_1(a)$. Expanding $g(a\,\cos\,\psi+U_{\rm dc})$ around $U_{\rm dc}$, it follows that

$$A_1(a)=\frac{a}{2}\left[g(U_{\rm dc})+D+\frac{a^2}{8}g''(U_{\rm dc})+\cdots\right]. \tag{12}$$

The expression for A_1 can qualitatively be derived from Eq. (4) in the following way. Multiplying Eq. (4) with V the left-hand side can be written as $d/d\tau(\dot{V}^2+V^2)$. This is the rate of change of the total energy if V is considered the coordinate of a particle in the harmonic potential V^2. It is small as long as ϵ is small. Here it represents the rate of change of the energy stored in the capacitance and the inductance. With $V=a(\tau)\cos\,\tau$ and $\dot{V}=a(\tau)\sin\,\tau+\dot{a}\cos\,\tau$, we average the equation over one period assuming that a and its derivative are constant over the period. Then higher-order derivates of a are neglected, since a is assumed to vary slowly, and we get

$$\frac{d}{d\tau}\frac{a^2}{2}=-\frac{\epsilon a^2}{2\pi}\int_0^{2\pi}[g(a\,\cos\,\psi+U_{\rm dc})+D]\sin^2\,\psi\,d\psi \tag{13}$$

which gives $\dot{a}=\epsilon A_1$ with A_1 given by Eq. (11).

A kinetic model of the current-voltage characteristic based on the existence of a current-limiting-potential minimum between the double layer and S_1 has been presented in Ref. [8]. To get a good agreement between the measured amplitude characteristics and those predicted by the above theory, the normalized conductance of the plasma column is approximated here by a least-squares fit of the form

$$g(U)\approx\frac{1}{V_1-V_2}\left[V_2\,\exp\left(-\frac{U-U_m}{V_2}\right)-V_1\,\exp\left(-\frac{U-U_m}{V_1}\right)\right]. \tag{14}$$

For $V_1>V_2$, $g(U)$ has a minimum at $U=U_m$ as required and $g(U_m)=-1$ for any value of the constants V_1 and V_2. It follows that

$$A_1(a)=-\frac{1}{V_{1-V_2}}\left[V_2^2\,\exp\left(-\frac{V_b}{V_2}\right)I_1\left(\frac{a}{V_2}\right)-V_1^2\,\exp\left(-\frac{V_b}{V_1}\right)I_1\left(\frac{a}{V_1}\right)\right]-\frac{D}{2}a, \tag{15}$$

where I_1 is a modified Bessel function of the first kind and V_b is defined by $V_b=U_{\rm dc}-U_m$. From the static current-voltage characteristic R_m has been determined to be 1950 Ω with a maximum error of 100 Ω. The uncertainty in R_m is due to the fact that the time-averaged current I shows a standard deviation of approximately 1 mA because of fluctuations in the plasma. Fitting $\int g(U)dU/R_m+I_0$ to the measured static current-voltage characteristic, when R_m

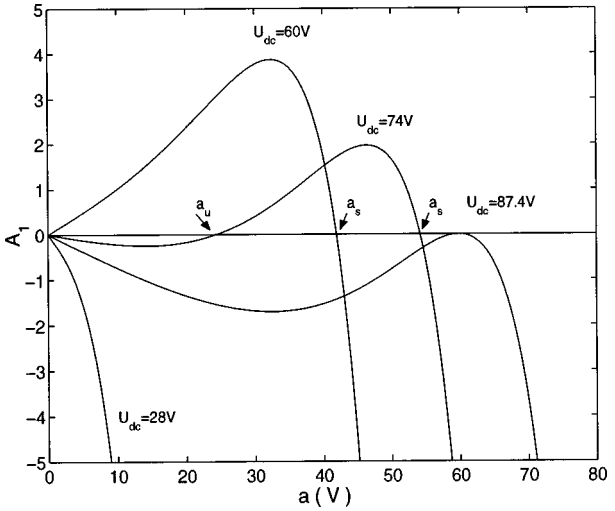

FIG. 6. A_1 (a)$=\dot{a}/\epsilon$ for $D=0.220$ evaluated according to Eq. (11) for different dc voltages $U_{\rm dc}$. For $U_{\rm dc}<U_1=29.5$ V, the only stationary oscillation amplitude, given by the roots of A_1, is $a=0$ (Fig. 2). For $U_1<U_{\rm dc}<U_3=87.4$ V a stable stationary amplitude a_s exists. At $U_{\rm dc}=U_2=69.8$ V an additional root a_u corresponding to an unstable oscillation appears. The interval (U_2,U_3), where a_u exists, is the width of the hysteresis. At its upper end the oscillation amplitude collapses from $a=a_s=a_u$ to zero. The hysteresis appears only for $D<0.75$ because a_u exists only if the curvature of $g(U_{\rm dc})$ is negative in an interval around U_2.

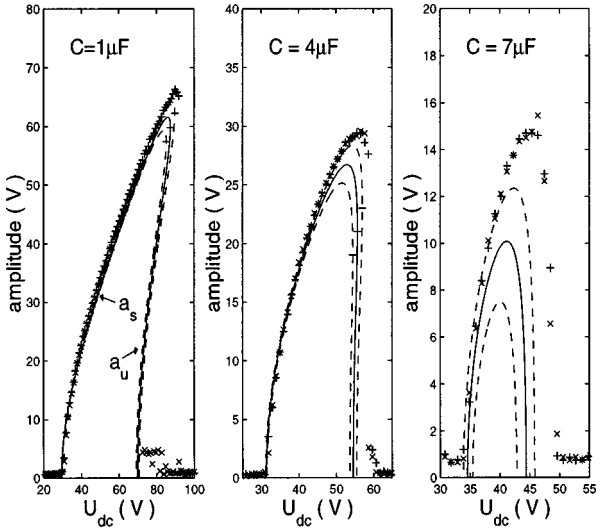

FIG. 7. Comparison between measured amplitudes (+, $U_{\rm dc}$ increasing; ×, $U_{\rm dc}$ decreasing) and amplitudes given by the roots of $A_1(a)=0$ (solid line) with $R_m=1950\ \Omega$ and $g(U_{\rm dc})$, according to Fig. 2 for $C=1$, 4, and 7 μF. The dashed lines give the uncertainty according to the 5% error in R_m. The theoretical amplitudes reproduce the transition from continuous to asymmetric characteristics containing hysteresis. The difference between them and the experimental amplitudes at $C=7$ μF is due to the overestimation of the damping by the fit function for $g(U_{\rm dc})$ for small values of $U_{\rm dc}$ (Fig. 2).

$=1950\ \Omega$ and I_0 is the plasma current at high dc voltages, we get $V_1=14.6$ V, $V_2=7.2$ V, and $U_m=38.7$ V [Fig. 2(b)].

V. DISCUSSION

The behavior of A_1 can be understood from the shape of $g(U_{\rm dc})+D$. Figure 6 shows A_1 according to Eq. (11) with $D=0.220$ for some values of $U_{\rm dc}$. For this D value, the interval (U_1,U_2), where $g(U_{\rm dc})+D<0$, is given by (29.5 V, 69.8 V). For $U_{\rm dc}<U_1$, the only root of A_1 is zero. Small fluctuations in V are damped, because $(d/da)A_1(a)|_{(a=0)}=-[g(U_{\rm dc})+D]/2$ is negative [Eq. (12)]. Oscillations are not excited and the double layer is stable. When $U_1<U_{\rm dc}<U_2$, any small deviation from $a=0$ will grow until the oscillation resides long enough in the region where $g(U_{\rm dc})+D>0$ to balance energy production and energy dissipation. A_1 then has one extra root a_s (Fig. 6, $U_{\rm dc}=60$ V). The negative slope of A_1 at $a=a_s$ shows that a_s is a stable oscillation amplitude because $\dot{a}>0$ for $a<a_s$, so that a grows, and $\dot{a}<0$ for $a>a_s$, so that the oscillation is damped until a reaches a_s.

For the D value considered in Fig. 6, this stable oscillation amplitude a_s still exists in the interval $U_2<U_{\rm dc}<U_3$ with $U_3=87.4$ V. A_1 now has an additional root $a=a_u$ in this interval [Fig. 6, $U_{\rm dc}=74$ V]. Clearly a_u does not correspond to a stable oscillation amplitude. For amplitudes below a_u, damping will bring a to zero and amplitudes above a_u, will grow up to the stable amplitude a_s. As discussed below, the appearance of a_u at $U_{\rm dc}=U_2$ is connected with the fact that the curvature of $g(U_{\rm dc})$ is negative in a region around $U_{\rm dc}=U_2$. With increasing a, the negative curvature causes the energy production to increase faster than the dissipation and it can balance the latter at $a=a_u$.

Since $A_1(a)$ is negative in $(0,a_u)$, the oscillation can therefore no longer be self-excited from small values of a. However, if the oscillation that is already excited, it will persist because $A_1(a)>0$ in (a_u,a_s). As $U_{\rm dc}$ is increased above U_2, the interval (a_u,a_s) gets smaller until $a_u=a_s$ at $U_{\rm dc}=U_3$. Then $A_1(a)$ is negative for any value of a and the oscillation suddenly disappears. If instead $U_{\rm dc}$ is decreased from large values, for which $a=0$, oscillations are not excited until they become self-excited at $U_{\rm dc}=U_2$. The amplitude characteristic therefore undergoes a hysteresis when $U_{\rm dc}$ is changed slowly. This is in agreement with the experiments.

For increasing D the interval (U_2,U_3) gets smaller. Hysteresis is obtained as long as a_u, exists. When $U_{\rm dc}$ is close to U_2, that is, when $g(U_{\rm dc})+D$ is close to zero, a small amplitude expansion, given by the first two terms of Eq. (12), is valid, and we get

$$a_u=2\sqrt{-\frac{2[g(U_{\rm dc})+D]}{g''(U_{\rm dc})}}. \tag{16}$$

For $U_{\rm dc}>U_2$ and $g''(U_{\rm dc})<0$, this root corresponds to a stationary but unstable oscillation with small amplitude. Hysteresis will accordingly appear only if $g''(U_{\rm dc})<0$. The transition from amplitude characteristics containing the amplitude collapse to continuous ones takes place when $g(U_2)=0$. For the experimental data it follows that $g''<0$ for $U_{\rm dc}>48.7$ V, so that we must have $D<0.75$ and $C<4.6\pm0.5$ μF for the hysteresis to occur. This result fits well with the observation (Fig. 5). The collapse of the

double-layer oscillation at $U_{dc}=U_3$ is caused by the fact that for $U_{dc}>U_3$ the dissipation in the outer circuit cannot be balanced any longer by the limited region of energy production. Without external dissipation $(R=0)$, the oscillation amplitude would grow approximately linearly with U_{dc}, and an amplitude collapse would not be observed.

Figure 7 shows the amplitude characteristics for $C=1$, 4, and 7 μF, and the roots of A_1 with ϵ and D values according to Table I. The 5% error in the estimation of R_m causes an uncertainty in the values of ϵ and D, as indicated by the dashed lines. The theoretical amplitudes show good agreement with the measured ones. They are, in general, smaller than the measured ones because the fit to g according to Eq. (14) overestimates the differential conductance of the plasma for small U_{dc} [Fig. 2(a)]. This results in too-large damping and smaller stationary oscillation amplitudes.

The type of instability we describe is expected to exist, in general, in current-carrying plasmas with strong double layers and not-too-large damping in the external circuit. Any increase in the applied potential drop and the double-layer potential drop will lead to a decrease in the density and the electric current in the plasma on the low-potential side. Through the external circuit, the current decrease increases the applied voltage drop, thereby resulting in a further decrease of the electric current. Only if the external circuit only consists of an electromotive force, the instability is not active, since the feedback will then vanish. The nonlinear evolution of the instability may be different in different types of plasmas. In our case it leads to virtual cathode oscillations, which are controlled by the double-layer potential drop. When L/C is large, the oscillation appears as sharp current disruptions. These give rise to high inductive overvoltages supported by the double layer. In this manner, the magnetic energy, stored in the inductance, is released as particle energy in the double layer [7]. A similar mechanism for energy release and particle acceleration by double layers in cosmic plasmas (e.g., solar flares) has been discussed in Ref. [23].

VI. SUMMARY

We have shown experimentally that the amplitude characteristics of double-layer oscillations go through a transition from continuous shapes, as seen with the classical van der Pol oscillator, to asymmetric shapes, including sudden amplitude jumps and hysteresis. The latter are not predicted by the classical van der Pol equation. A generalized van der Pol equation, based on the static current-voltage characteristic of the double layer in the experiment, is derived for the system. Solutions are obtained by an asymptotic method for weak nonlinearity developed by Mitropolsky and Bogoliubov. The solution fully explains the observed transition of the amplitude characteristics and the amplitude jumps, which may be as large as 70% of the dc voltage drop across the double layer. The collapse of the oscillation is caused by damping, resulting from resistive power consumption in the external circuit.

ACKNOWLEDGMENT

This work was supported by the Swedish National Science Research Council.

[1] P. Burger, J. Phys. D **36**, 1938 (1965).
[2] W. Otta, Z. Naturforsch. **22**, 1057 (1967).
[3] S. Iizuka, P. Michelsen, J. J. Rasmussen, R. Schrittwieser, and R. Hatakeyama, Phys. Rev. Lett. **48**, 145 (1982).
[4] F. Bauer and H. Schamel, Physica D **54**, 235 (1992).
[5] F. Greiner, T. Klinger, H. Klostermann, and A. Piel, Phys. Rev. Lett. **70**, 3071 (1993).
[6] R. T. Carpenter and S. Torvén, IEEE Trans. Plasma Sci. **15**, 434 (1987).
[7] S. Torvén, L. Lindberg, and R. T. Carpenter, Plasma Phys. Controlled Fusion **27**, 143 (1985).
[8] T. Klinger, A. Piel, I. Axnäs, and S. Torvén, Phys. Scr. **56**, 70 (1997).
[9] U. Parlitz and W. Lauterborn, Phys. Rev. Lett. **36**, 1428 (1987).
[10] R. Mettin, U. Purlitz, and W. Lauterborn, Int. J. Bifurcation Chaos Appl. Sci. Eng. **3**, 1529 (1993).
[11] H. Lashinsky, *Symposium on Turbulence of Fluids and Plasmas* (Polytechnic Press, Brooklyn, NY, 1968).
[12] P. Michelson, H. L. Pécseli, J. J. Rasmussen, and R. Schrittwieser, Plasma Phys. Controlled Fusion **21**, 61 (1979).
[13] T. Gyergyek, M. Cercek, N. Jelic, and M. Stanojevic, Contrib. Plasma Phys. **33**, 53 (1993).
[14] M. Koepke, M. J. Alport, T. E. Sheridan, W. E. Amatucci, and J. J. Caroll III, Geophys. Res. Lett. **21**, 1011 (1994).
[15] T. Klinger, F. Greiner, A. Rohde, and M. Koepke, Phys. Rev. E **52**, 4316 (1995).
[16] M. Koepke and D. M. Hartley, Phys. Rev. A **44**, 6877 (1997).
[17] I. Axnäs, S. Torvén, T. Klinger, and A. Piel, in *Proceedings of the International Conference on Plasma Physics, Nagoya, Japan, 1996*, edited by H. Sugai and T. Hayashi (The Japan Society of Plasma Science and Nuclear Research, Nagoya, 1997).
[18] B. van der Pol, Philos. Mag. **43**, 700 (1922).
[19] N. N. Bogoliubov and Y. A. Mitropolsky, *Asymptotic Methods in the Theory of Non-Linear Oscillations* (Hindustan Publishing Corp., Delhi, 1961).
[20] M. A. Raadu and J. J. Rasmussen, Astrophys. Space Sci. **144**, 43 (1988).
[21] M. A. Raadu, Phys. Rep. **178**, 25 (1989).
[22] S. Iizuka, P. Michelsen, J. J. Rasmussen, R. Schrittwieser, R. Hatakeyama, K. Saeki, and N. Sato, J. Phys. Soc. Jpn. **54**, 2516 (1985).
[23] P. Carqvist, IEEE Trans. Plasma Sci. **PS-14**, 794 (1986).